Title

Reformulated McNamara RBE-weighted beam orientation optimization for intensity modulated proton therapy

Journal

Medical Physics, 49(4)

ISSN

0094-2405

Authors

Ramesh, Pavitra
Lyu, Qihui
Gu, Wenbo
et al.

Publication Date

2022-04-01

DOI

10.1002/mp.15552

Peer reviewed

HHS Public Access

Author manuscript

Med Phys. Author manuscript; available in PMC 2023 February 02.

Published in final edited form as:

Med Phys. 2022 April ; 49(4): 2136–2149. doi:10.1002/mp.15552.

Reformulated McNamara RBE-weighted Beam Orientation Optimization for Intensity Modulated Proton Therapy

Pavitra Ramesh[1], **Qihui Lyu**[1], **Wenbo Gu**[2], **Dan Ruan**[1], **Ke Sheng**[1]

[1]Department of Radiation Oncology, University of California Los Angeles, Los Angeles, CA 90095, USA

[2]Department of Radiation Oncology, University of Pennsylvania, Philadelphia, PA 19104, USA

Abstract

Purpose: Empirical relative biological effectiveness (RBE) models have been used to estimate the biological dose in proton therapy but do not adequately capture the factors influencing RBE values for treatment planning. We reformulate the McNamara RBE model such that it can be added as a linear biological dose fidelity term within our previously developed sensitivity-regularized and heterogeneity-weighted beam orientation optimization (SHBOO) framework.

Methods: Based on our SHBOO framework, we formulated the biological optimization problem to minimize total McNamara RBE dose to OARs. We solve this problem using two optimization algorithms: FISTA (McNam-FISTA) and Chambolle-Pock (McNam-CP). We compare their performances with a physical dose optimizer assuming RBE=1.1 in all structures (PHYS-FISTA) and an LET-weighted dose model (LET-FISTA). Three head and neck patients were planned with the four techniques and compared on dosimetry and robustness.

Results: Compared to Phys-FISTA, McNam-CP was able to match CTV [HI, Dmax, D95%, D98%] by [0.00, 0.05%, 1.4%, 0.8%]. McNam-FISTA and McNam-CP were able to significantly improve overall OAR [Dmean, Dmax] by an average of [36.1%,26.4%] and [29.6%, 20.3%], respectively. Regarding CTV robustness, worst [Dmax, V95%, D95%, D98%] improvement of [−6.6%, 6.2%, 6.0%, 4.8%] was reported for McNam-FISTA and [2.7%, 2.7%, 5.3%, −4.3%] for McNam-CP under combinations of range and setup uncertainties. For OARs, worst [Dmax, Dmean] were improved by McNam-FISTA and McNam-CP by an average of [25.0%, 19.2%] and [29.5%, 36.5%], respectively. McNam-FISTA considerably improved dosimetry and CTV robustness compared to LET-FISTA, which achieved a better worst-case OAR doses.

Conclusion: The four optimization techniques deliver comparable biological doses for the head and neck cases. Beside modest CTV coverage and robustness improvement, OAR biological dose and robustness were substantially improved with both McNam-FISTA and McNam-CP, showing potential benefit for directly incorporating McNamara RBE in proton treatment planning.

Corresponding author: Ke Sheng, Ph.D., UCLA Radiation Oncology, 200 Medical Plaza Driveway, Los Angeles, CA, 90095, USA, ksheng@mednet.ucla.edu.

Conflicts of Interest

The authors have no relevant conflicts of interest to disclose.

Keywords

Proton therapy-dose optimization; RBio-Particle therapy-Protons; RBE

I. Introduction

The linear energy transfer (LET) of protons is 1–2 orders of magnitude greater than MV X-rays and vary substantially with depth. The greater LET values have been conventionally accounted for using a generic relative biological effectiveness (RBE) of 1.1 in proton radiotherapy planning[1]. However, related to the variable LET values, studies have shown that RBE is not spatially invariant across the spread-out Bragg peak (SOBP) region[2]. Besides LET, the RBE values are further compounded by factors including cell alpha-beta ratio, physical dose, cell type and biological endpoints[3–5]. Using generic RBE in treatment planning may lead to inaccurate estimation of the biological affects and increased toxicity to adjacent critical structures[6]. Patients with tumors at intricate anatomies and close proximity to radiosensitive organs, i.e., the head and neck region, are particularly vulnerable to the inaccuracy[7,8]. These concerns motivated more accurate modeling of proton RBE and incorporation of the variable RBE into treatment planning.

Several empirical RBE models have been proposed to improve the calculation of RBE in human tissue[9–12]. Amongst these models, the McNamara model is fitted from extensive *in vitro* cell survival datasets published through 2015, making it one of the most comprehensive proton RBE models for treatment planning and optimization[12]. However, inverse optimization incorporating McNamara type of RBE is not straightforward due to its dependence on both the physical dose and LET-weighted dose. The non-linearity of the cost function renders typical optimization methods impractical. The RBE optimization problem is further complicated by the robustness consideration. As simplification, several alternative optimization problems were solved. First, LET or LET weighted dose distribution was used as a surrogate for McNamara RBE-weighted dose distribution[13–18]. Second, the optimization problem was divided into subproblems calculating McNamara RBE, physical dose, and LET separately. The RBE dose was evaluated at the end of treatment planning[19,20] or sequentially in an iterative process[21], which does not promise problem convergence.

Another often overlooked factor influencing proton planning is the beam orientation selection. Compared with manually selecting beam orientations, we have shown that inverse optimization with a group sparsity term can more thoroughly search through the beam space for both superior physical dosimetry[22] and robustness[23]. Because the beam orientation separately affects the plan RBE due to the RBE variation along the beam direction, integrating RBE into the beam orientation optimization (BOO) framework would help select beams that are both dosimetrically and biologically desirable. To demonstrate the benefit, we previously studied LET weighted proton planning with BOO[24]. We showed that compared with manually selected beams, including LET substantially reduced the OAR LET weighted doses.

As a logical extension of previous research, in this study, we employ the same BOO framework for the RBE-weighted dose optimization problem. We reformulate the empirical

McNamara model into a single and mathematically tractable optimization problem such that the biological detail of the fitting parameters is preserved. A robustness analysis is also performed to assess the plan robustness with varying RBE considerations.

II. Materials and Methods

The general goal of our IMPT McNamara RBE-based BOO algorithm is to select 2–4 beams out of all candidate beams and simultaneously generate a robust fluence map that minimizes biological dose in the OARs while maintaining dose to the target, all while achieving sufficient physical dose distribution.

A. RBE-weighted Dose Fidelity

In a typical inverse optimization problem, we set the initial biological dose fidelity as

$$\Gamma(Ax) = \sum_{i \in \mathcal{T}} \omega_i \| RBE_i(\boldsymbol{x}) \cdot D_i - q_i \|^2 + \sum_{i \in \mathcal{O}} \omega_i \| RBE_i(\boldsymbol{x}) \cdot D_i - m_i \|_+^2, \quad (1)$$

where fluence map $\boldsymbol{x}$ is the optimization variable, dose is $D_i = \sum_j a_{ij} x_j$ and dose-averaged LET is $LETd_i = \frac{1}{D_i} \sum_j l_{ij} a_{ij} x_j$. The dose calculation matrix A includes all candidate beams, with each column being the vectorized doses delivered from one intensity spot to its surrounding voxels. The LET calculation matrix, L, is calculated similarly to dose matrix A for vectorized LET-weighted dose. The phenomenological McNamara model is used to calculate RBE values for protons in each voxel and is formulated as

$$RBE\left(D, \left(\frac{\alpha}{\beta}\right)_x, LET_d\right) = \frac{1}{2D} \left(\sqrt{\left(\frac{\alpha}{\beta}\right)_x^2 + 4D\left(\frac{\alpha}{\beta}\right)_x \left(p_0 + \frac{p_1}{(\alpha/\beta)_x} LET_d\right) + 4D^2 \left(p_2 + p_3 \sqrt{(\alpha/\beta)_x} LET_d\right)^2} - \left(\frac{\alpha}{\beta}\right)_x \right) \quad (2)$$

. The fit coefficients are p0=0.99064 (Standard Error (SE) 0.014125), p1=0.35605 (SE 0.015038), p2=1.1012 (SE 0.0059972), and p3=−0.0038703 (SE 0.00091303)[12]. Without losing generality, the alpha-beta ratio values from reference photons $\left(\frac{\alpha}{\beta}\right)_x$ were assigned 10 Gy in the target volumes and 3 Gy in the surrounding normal tissues.

The first term minimizes the difference between the RBE-weighted dose to the target volumes $\mathcal{T}$ and the prescribed biological dose (GyRBE) q; the second one-sided quadratic term minimizes dose to OAR $\mathcal{O}$, where m is the maximum allowable biological dose (GyRBE) in that structure. Individual structure tuning is controlled by weights ω_i. CTV volumes were assigned highest priority.

However, this optimization problem is difficult to solve since (2) also depends on optimization variable $\boldsymbol{x}$. We propose an alternative approach for incorporating the McNamara model within the optimization framework.

B. Reformulated McNamara RBE-Weighted Dose Fidelity

The alternative approach attempts to optimize the total dose in each structure. In inverse optimization schemes, the objective function is formulated to account for minimum and maximum dose constraints to the target and for maximum dose constraints to the organs at risk (OARs)[13]. Since it would be difficult to satisfy both maximum and minimum total dose constraints in the target volume without loss of homogeneity, the following approach assumes previously calculated values of RBE (via physical dose optimization), which are static during the CTV biological dose optimization, and for OARs, a direct reduction of biological dose using reformulated McNamara RBE values. The McNamara model can be written more simply as

$$(RBE \times D)_i = \frac{1}{2}\sqrt{a_1 + a_2 D_i + a_3 (LET \times D)_i + (a_4 D_i + a_5 (LET \times D)_i)^2} + a_6 \tag{3}$$

, where a_1-a_6 are constants derived from parameters in the McNamara model. For OARs, minimization of (1) can be equivalently achieved by minimizing the following function $f_i(x)$,

$$f_i(x) = a_1 + a_2 D_i x + a_3 (LET \times D)_i x + (a_4 D_i x + a_5 (LET \times D)_i x)^2 \tag{4}$$

Summing over all voxels, we obtain a new set of biological dose fidelity terms for OARs in (5). $\vec{c}$ is the sum over the columns of matrix $a_2 D_i + a_3 (LET \times D)_i$ and H is simply $a_4 D_i + a_5 (LET \times D) i$.

$$f(x) = \sum_i f_i(x) = \vec{c}\, x + \|Hx\|_2^2 + \text{constant} \tag{5}$$

The optimization problem is then extended in (6) to include our previously formulated sensitivity and heterogeneity weighted group sparsity terms,

$$\begin{aligned} \text{minimize}_x\ & \underbrace{\vec{c}\,\boldsymbol{x} + \|H\boldsymbol{x}\|_2^2}_{OAR\ RBE\ term} + \underbrace{\|RBE \cdot A\boldsymbol{x} - d\|_2^2}_{Static\ RBE\ dose\ for\ CTV} + \underbrace{\sum_{b \in \beta} \alpha_b h_b \|\boldsymbol{x}_b\|_2^{\frac{1}{2}}}_{group\ sparsity\ term} \\ & + \underbrace{\sum_{k \in \{u,v\}} \lambda_k \boldsymbol{s}_k^T \boldsymbol{x}}_{sensitivity\ term}, \quad subject\ to\ \ \boldsymbol{x} \geq 0 \end{aligned} \tag{6}$$

where $\boldsymbol{x}_b$ is a vector representing the intensities of scanning spots from the candidate beam b, so optimization variable $\boldsymbol{x}$ is the concatenation of all vectors $\boldsymbol{x}_b$ ($b \in \beta$). The third term is an L2,1/2-norm group sparsity term. A proper value of weighting hyperparameter α_b is set for each beam, defined as

$$\alpha_b = z\left(\frac{\left\|A_{CTV}^b \vec{1}\right\|_2}{n_b}\right)^{p/2} \tag{7}$$

, where A_{CTV}^b is the dose calculation matrix of the target volume for beam b, n_b is the number of candidate spots in beam b, and z is a regularization parameter. This weight ensures that most beams are penalized to be identically zero, turning most candidate beams

off, and leaving a small number (2–4) of beams active. Parameter z is tuned higher to further force convergence to a smaller number of active beams. The lateral tissue heterogeneity observed along beam b is represented by its heterogeneity index h_b, choosing beams with less sensitivity to setup uncertainties. The fourth term is a sensitivity regularization term, where λ_k is a regularization parameter, $\boldsymbol{s_u}$ and $\boldsymbol{s_v}$ are longitudinal and lateral sensitivity vectors that account for range uncertainties for each spot in each beam, both in the beam direction (**u**) and perpendicular to the beam (**v**)[25].

FISTA, an accelerated proximal gradient method known as the Fast-Iterative Shrinkage Thresholding Algorithm[26], or Chambolle-Pock, a primal-dual algorithm[27], are used to solve this non-differentiable problem. Both proximal gradient and first order primal dual methods have efficiently solved inverse optimization problems with applications to treatment planning in the past[28,29] and are straightforward to implement for large scale, nondifferentiable, constrained convex optimization problems using a faster line-search method. Other algorithms like the alternating direction method of multipliers (ADMM)[30] must solve a large linear system at each iteration, while algorithms like CP and FISTA require only matrix-vector multiplications[31]. Compared with CP with convergence rate of $O(1/k^2)$ FISTA is faster because of its high convergence rate of $O(1/k^2)$[26]. On the other hand, for non-convex problems such as the one at hand, CP may find a better local minimum[32]. Therefore, both solvers are studied here. The solution for the FISTA method can be found in our previous work[33] and the CP method is described in Section S1.

C. Comparison with LET-Weighted Dose Fidelity

The above McNamara formulation is compared with our previously developed LETwBOO framework[24] to determine the efficacy of integrating RBE into proton treatment planning. Using the same SHBOO-FMO basis, the LET-weighted optimization problem is

$$\begin{aligned}&\text{minimize}_x \sum_{i\in\mathcal{T}}\omega_i\|D_i-q_i\|^2+\sum_{i\in\mathcal{O}}\omega_i\|D_i-m_i\|_+^2\\&+\sum_{i\in\mathcal{T}}\omega_i\left\|LETd_i\cdot D_i-(LD)_i^{ref}\right\|^2+\sum_{i\in\mathcal{O}}\omega_i\|LETd_i\cdot D_i\|_+^2\\&+\sum_{b\in\beta}\alpha_b h_b\|\boldsymbol{x}_b\|_2^{\frac{1}{2}}+\sum_{k\in\{u,v\}}\lambda_k\boldsymbol{s}_k^T\boldsymbol{x}\ \textit{subject to}\quad \boldsymbol{x}\geq 0\end{aligned}\tag{9}$$

The first two terms represent conventional physical dose fidelity and the third and fourth terms represent the LET × D conditions. $(LD)_i^{ref}$ is the minimum LET-weighted dose in the CTV to prevent cold spots in the biological dose. It was evaluated as the mean LET-weighted dose from conventional plans optimizing physical dose with manually selected beams. This problem was solved using FISTA.

D. Patient Evaluations

Three bilateral head-and-neck (HN) patients were tested. The original candidate beam set of 1162 non-coplanar beams was evenly distributed across a 4π space with 6° separation. A subset of about 220 beams were used for the head and neck patients, the rest excluded due to infeasible depths, undesired entrance through incompletely segmented vital organs as

a result of limited CT range, or collisions between the proton nozzle and patient or couch. All beams were tested for collision using 3D visualizations of STL files of the IBA Proteus Plus gantry with PBS-dedicated nozzle, scissor couch, and each of the patient masks[34]. A range shifter was added to degrade the proton range to treat at superficial depths[35]. The dose loading matrix A and LET matrix L were calculated using matRad v2.1.0[36,37], a MATLAB-based 3D treatment planning toolkit, describing the dose and LET from the scanning spots covering the CTV and a 5 mm margin to a voxels of resolution 2.5 × 2.5 × 2.5 mm^3. Energies are interpolated in matRad to achieve a uniform layer spacing of 3 mm in the beam direction, and the spot spacing in the lateral direction was 5 mm (please refer to matRad documentation for more information on dose influence matrix calculation). The CTV was set as the optimization target and CTV-based robust optimization was performed. The prescription dose, target volume, and average number of spots per beam for each patient are shown in Table I.

Three plans were created for each patient, all of them including group sparsity-based beam orientation optimization (SHBOO): 1) optimization of physical dose using the FISTA algorithm (Phys-FISTA); 2) optimization of the reformulated McNamara RBE-weighted dose using FISTA (McNam-FISTA); 3) optimization of the reformulated McNamara RBE-weighted dose using Chambolle-Pock (McNam-CP). A separate analysis is conducted with a fourth plan that was created for all three patients: 4) optimization of LET-weighted dose using FISTA (LET-FISTA), for direct comparison against McNam-FISTA. For each patient, all four plans were optimized using the same structure weighting. All plans are optimized using their respective biological dose fidelity terms. Once all optimizations were completed and fluence maps were obtained, final RBE dose (GyRBE) for each plan was calculated using (3) and compared.

Plans were normalized such that 95% of the target volumes received the prescribed dose. CTV homogeneity, D95%, D98%, and maximum dose were evaluated. CTV homogeneity is defined as D95% /D5%. The maximum dose is defined as the dose to 2% of the structure volume, D2%, following the recommendation by ICRU-83[38]. The mean and maximum doses for OARs were also evaluated. The robustness analysis considered twenty-one scenarios: a result of all combinations of (a) two range uncertainty worse-case scenarios, by scaling the CT number ± 3% and (b) six setup uncertainty worst-case scenarios, by shifting the beam isocenter by ± 3 mm along anteroposterior, superior-inferior, and mediolateral directions. The range and setup uncertainties were combined in the robustness analysis since they are not mutually exclusive. The robustness of each plan was evaluated by the DVH band plots[39]. Worst Dmax, D98%, D95%, and V95% for each CTV and worst Dmean and Dmax for OARs were calculated between plans.

III. Results

A. Runtime and Selected Beams

The dose, sensitivity and heterogeneity calculation for all candidate beams were performed with MATLAB and the Parallel Computing Toolbox on an i7 12-core CPU desktop. The average time per beam to calculate this data, along with the total beam orientation with fluence map optimization runtime for Phys-FISTA, McNam-FISTA, McNam-CP, and LET-

FISTA for each patient is listed in Table II. Dose calculation among patients used the same ray-tracing procedure in matRad for the same number of candidate beams[24]. Lateral tissue heterogeneity index values of all scanning spots in the same beam are calculated and averaged to represent the beam heterogeneity, adding more time to initial calculation[23]. The McNam-FISTA and McNam-CP plans increased the total optimization time by 130–410% and 400–1370%, respectively, compared to Phys-FISTA. Since both McNamara plans use extra terms in their objective functions to accurately represent biological dose fidelity, it is understood that total optimization time increases. There is an 8–350% increase in runtime between FISTA and CP. Even with a higher regularization parameter z, CP struggled to produce less than 4 beams during beam selection. The increase can also be attributed to the fact that computation of additional proximal operators was necessary for reformulating the objective function into the CP standard form. McNam-FISTA increased optimization time on average by 11% compared to LET-FISTA.

The couch and gantry angles for the beams for each case are listed in Table III. The angle notation follows IEC 61217 coordinate conventions. A three-dimensional portrayal of beam angles selected are shown in Figure 1.

B. Patient Dosimetry

The dosimetric features across plans can be seen in Figure 2. Dose maps for each patient are normalized to the same biological dose for clear comparison. Compared to Phys-FISTA, CTV homogeneity index (HI) and maximum biological dose (Dmax) are either matched or improved by McNam-CP by an average of 0.00 and 0.05% of the prescription dose, respectively. McNam-FISTA did not improve the CTV homogeneity as shown by an average decline of 0.02 and 8.2% for HI and Dmax compared to Phys-FISTA. D95% and D98% are changed by McNam-FISTA and McNam-CP by [−3.5%, −0.3%] and [1.4%,0.8%] of the prescription dose, respectively, compared to Phys-FISTA. CTV statistics for the three patients are listed in Table IV.

All RBE-weighted plans met the dosimetric standards set during optimization. Generally, relatively large improvement could be seen in the mean and maximum biological doses of all structures with the McNamara plans compared to the physical dose plan. Table V reports these dose statistics for all structures. [Dmean, Dmax] (GyRBE) were improved by [−1.8, 7.3] in the right submandibular gland, [1.7, 1.8] for the left parotid, [4.6, −2.0] for the right parotid, [4.0, 11.5] in the larynx, [2.3, 6.4] for constrictors, [4.5, 19.5] in the esophagus, and [5.1, 36.2] in the spinal cord for McNam-FISTA, with negative values representing better performance with Phys-FISTA. Similarly, [Dmean, Dmax] (GyRBE) were improved by [2.9, 7.4] in the right submandibular gland, [2.1, 0.8] for the left parotid, [4.5, −0.6] for the right parotid, [1.8, 5.2] in the larynx, [0.3, −1.1] for constrictors, [4.3, 19.5] in the esophagus, and [5.1, 36.2] in the spinal cord for McNam-CP. Biological dose volume histograms for the three H&N patients are shown in Figure 3.

C. Plan Robustness

All plans were optimized to account for uncertainties in range and setup due to sensitivity regularization and heterogeneity weighting. The DVH bands of the three methods are shown

in Figure 4. CTV robustness was improved for both McNam-FISTA and McNam-CP. Under range and setup uncertainties, narrower DVH bands, showing superior robustness, were generally observed with the McNam-CP plans for OARs compared to Phys-FISTA. McNam-FISTA also managed to provide comparable OAR robustness to Phys-FISTA plans.

The worst (highest) Dmax, and worst (lowest) V95%, D95%, and D98% of each CTV were calculated and plotted in Figure 5. On average, the worst [Dmax, V95%, D95%, D98%] improved by [−6.6%, 6.2%, 6.0%, 4.8%] with McNam-FISTA and [2.7%, 2.7%, 5.3%, −4.3%] with McNam-CP compared to Phys-FISTA. The worst Dmax and Dmean for each OAR under range and setup uncertainty combinations were calculated and plotted in Figure 6. The worst [Dmax, Dmean] was improved by McNam-FISTA and McNam-CP by an average of [25.0%, 19.2%] and [29.5%, 36.5%], respectively.

D. McNamara RBE Comparison with LET

Tumor coverage and normal tissue sparing with McNam-FISTA plans were compared directly to LET-FISTA plans for all patients as well. McNam-FISTA was able to improve tumor [HI, Dmax, D95%, D98%] by [0.08, 10.8%, −3.0%, 0.4%]. Average [Dmean, Dmax] (GyRBE) were improved by McNam-FISTA by [0.9, 9.8] in the right submandibular gland, [5.2, 8.2] for the left parotid, [8.6, 7.6] for the right parotid, [2.9, 4.4] in the larynx, [7.0, 16.0] for constrictors, [3.3, 12.3] in the esophagus, and [5.1, 36.2] in the spinal cord. Figure 7 shows a biological dose volume histogram comparison between plans for the three patients.

In terms of CTV robustness, the worst [Dmax, V95%, D95%, D98%] improved with McNam-FISTA compared to LET-FISTA by [26.2%, 21.1%, 19.9%, 37.0%] under range ad setup uncertainties. For OARs, however, the worst [Dmax, Dmean] was worsened by McNam-FISTA under uncertainties by an average of [2.3%, 4.4%]. The right-hand side of Figure 4 shows a biological DVH band plot representing the robustness comparison.

Although the McNamara model preserves the biological accuracy and preferentially spares OARs, the OAR sparing is less robust than the LET model. For CTVs, the McNamara model is more robust. This shows that for LET-FISTA, Bragg peaks are placed away from the distal edge of the CTV, giving a large range of RBE values within the tumor, showing a trade-off between dosimetry and robustness.

IV. Discussion

In this study, we have developed a framework that directly optimizes the McNamara RBE model, which comprehensively captures extensive proton cell survival datasets. We reformulated the phenomenological McNamara RBE equation for tractable optimization solution. Our method better preserves model details in optimization compared with previous studies using simplified RBE or LET surrogates. More importantly, the RBE is incorporated into the BOO framework that performs a global search among all feasible candidate beams for optimal physical and biological dose distribution. Compared with previous approaches appending RBE or LET optimization to the physical dose optimization the linear McNamara reformulation further reduces biological dose in OARs without loss of tumor coverage.

The alpha/beta values used in this study are generalized based on type of structure (OAR vs CTV) rather than specific cell line. However, these values directly impact the voxel-based McNamara RBE calculations for each method. A Monte Carlo robustness study has gathered the uncertainties listed for the McNamara model parameters and alpha/beta values from a variety of studies[40]. Uncertainties in tumor radiobiology and their varying endpoints propagate errors throughout the optimization, disrupting the accurate assessment of tissue toxicities. While further investigations are needed to better understand the radiobiology of proton therapy, a method improving biological effectiveness is a safe and clinically acceptable solution.

Because the main concern for the proton RBE is on normal organs[41,42], to formulate the RBE optimization problem for tractable solution, we focused our efforts on RBE-dose in the OAR structures. Since the OAR RBE term in (8) represents a minimization over the total dose in the structure volume, the goal for total dose can be 0 GyRBE if for all voxels the desired dose is 0 GyRBE. It is not as straightforward to optimize the total CTV dose around a set value if, in each voxel, the dose is then allowed to significantly vary from prescription dose. This would lead to inhomogeneity within the CTV. Although the reformulated method is not applied to the CTVs, McNamara RBE should still be incorporated into CTV dose optimization since *in vivo* RBE within large HN tumors may not be uniformly 1.1. Voxel-based RBE values for CTVs are therefore calculated via physical dose optimization prior to McNamara RBE-based optimization.

Because RBE values are largely dependent on LET values, the method calculation of LET values should be noted for this study. Due to the prohibitively long time required to calculate dose and LET for over 200 candidate beams using Monte Carlo, the current study used an analytical method for all patients. While the analytical method was shown to be acceptably accurate for dose calculation and BOO planning in our previous papers[22,23], it is limited in LET calculation accuracy due to reasons including failing to account for secondary protons[43]. The deficiency is shown as overestimation of LET in the low-density region compared with the Monte Carlo method. It is also observed that a different dose and LET calculation method can result in different optimized beams.

A comparison between optimization algorithms was performed using the same formulation for our objective function. The problem is efficient to solve using FISTA, which has an optimal convergence rate of $O(1/k^2)$ among first-order optimization methods[26]. The problem demands more time and computational power for Chambolle-Pock with convergence rate of $O(1/k)$. With the heterogeneity weight included in the group sparsity term, Chambolle-Pock was unable to select 2–4 beams within a reasonable time span. The weight was excluded during beam selection to force convergence. Although CP convergence rate is not optimal, because of the non-convexity of the optimization problem, the CP plans in some cases find a better local minimum and provide superior dosimetry compared to FISTA. The superior dosimetry can be attributed to effectively higher OAR RBE priority in CP without the heterogeneity index term. CP on average selects two more beams than FISTA plans, which may also explain the differences in results. Previous studies have shown improvement in dosimetry with three-angle plans over two-angle plans but no advantage with four-angle plans over three-angle plans[44,45].

Further research should be conducted to optimize both physical dose robustness towards geometrical and range uncertainties, and RBE robustness towards biological model parameter uncertainties. Biologically robust optimization algorithms that have thus far been proposed mostly consider worst case optimization[46–48], which would increase the computational burden of our current framework by at least 10 fold. Our sensitivity based robust planning method was able to handle physical dose robustness[23,25] of IMPT plans with minimal additional computational cost. Therefore, a future direction is to incorporate the biological uncertainties into sensitivity regularization.

V. Conclusions

We have developed a robust RBE-weighted beam orientation optimization method using direct reformulation of the McNamara phenomenological model. The proposed optimization framework markedly improved OAR RBE doses while maintaining similar physical dose distribution compared with the conventional method assuming a generic RBE value for all voxels.

Supplementary Material

Refer to Web version on PubMed Central for supplementary material.

Acknowledgement

This research is supported by NIH Grants No. R01CA230278.

References

1. McNamara A, Willers H, Paganetti H. Modelling variable proton relative biological effectiveness for treatment planning. Br J Radiol. 2019;93(1107):20190334. doi:10.1259/bjr.20190334 [PubMed: 31738081]
2. Ödén J, Toma-Dasu I, Witt Nyström P, Traneus E, Dasu A. Spatial correlation of linear energy transfer and relative biological effectiveness with suspected treatment-related toxicities following proton therapy for intracranial tumors. Med Phys. 2020;47(2):342–351. doi:10.1002/mp.13911 [PubMed: 31705671]
3. Mara E, Clausen M, Khachonkham S, et al. Investigating the impact of alpha/beta and LETd on relative biological effectiveness in scanned proton beams: An in vitro study based on human cell lines. Med Phys. 2020;47(8):3691–3702. doi:10.1002/mp.14212 [PubMed: 32347564]
4. Howard ME, Beltran C, Anderson S, Tseung WC, Sarkaria JN, Herman MG. Investigating Dependencies of Relative Biological Effectiveness for Proton Therapy in Cancer Cells. Int J Part Ther. 2018;4(3):12–22. doi:10.14338/IJPT-17-00031.1 [PubMed: 30159358]
5. Lühr A, von Neubeck C, Krause M, Troost EGC. Relative biological effectiveness in proton beam therapy - Current knowledge and future challenges. Clin Transl Radiat Oncol. 2018;9:35–41. doi:10.1016/j.ctro.2018.01.006 [PubMed: 29594249]
6. Buchsbaum JC, McDonald MW, Johnstone PAS, et al. Range modulation in proton therapy planning: a simple method for mitigating effects of increased relative biological effectiveness at the end-of-range of clinical proton beams. Radiat Oncol Lond Engl. 2014;9:2. doi:10.1186/1748-717X-9-2
7. Yuan TZ, Zhan ZJ, Qian CN. New frontiers in proton therapy: applications in cancers. Cancer Commun Lond Engl. 2019;39(1):61. doi:10.1186/s40880-019-0407-3

8. Kim JK, Leeman JE, Riaz N, McBride S, Tsai CJ, Lee NY. Proton Therapy for Head and Neck Cancer. Curr Treat Options Oncol. 2018;19(6):28. doi:10.1007/s11864-018-0546-9 [PubMed: 29744681]
9. Wedenberg M, Lind BK, Hårdemark B. A model for the relative biological effectiveness of protons: the tissue specific parameter α/β of photons is a predictor for the sensitivity to LET changes. Acta Oncol Stockh Swed. 2013;52(3):580–588. doi:10.3109/0284186X.2012.705892
10. Carabe-Fernandez A, Dale RG, Jones B. The incorporation of the concept of minimum RBE (RbEmin) into the linear-quadratic model and the potential for improved radiobiological analysis of high-LET treatments. Int J Radiat Biol. 2007;83(1):27–39. doi:10.1080/09553000601087176 [PubMed: 17357437]
11. Wilkens JJ, Oelfke U. A phenomenological model for the relative biological effectiveness in therapeutic proton beams. Phys Med Biol. 2004;49(13):2811–2825. doi:10.1088/0031-9155/49/13/004 [PubMed: 15285249]
12. McNamara AL, Schuemann J, Paganetti H. A phenomenological relative biological effectiveness (RBE) model for proton therapy based on all published in vitro cell survival data. Phys Med Biol. 2015;60(21):8399–8416. doi:10.1088/0031-9155/60/21/8399 [PubMed: 26459756]
13. Wilkens JJ, Oelfke U. Optimization of radiobiological effects in intensity modulated proton therapy. Med Phys. 2005;32(2):455–465. doi:10.1118/1.1851925 [PubMed: 15789592]
14. Bai X, Lim G, Grosshans D, Mohan R, Cao W. A biological effect-guided optimization approach using beam distal-edge avoidance for intensity-modulated proton therapy. Med Phys. 2020;47(9):3816–3825. doi:10.1002/mp.14335 [PubMed: 32557747]
15. Deng W, Yang Y, Liu C, et al. A Critical Review of LET-Based Intensity-Modulated Proton Therapy Plan Evaluation and Optimization for Head and Neck Cancer Management. Int J Part Ther. 2021;8(1):36–49. doi:10.14338/IJPT-20-00049.1
16. Traneus E, Ödén J. Introducing Proton Track-End Objectives in Intensity Modulated Proton Therapy Optimization to Reduce Linear Energy Transfer and Relative Biological Effectiveness in Critical Structures. Int J Radiat Oncol Biol Phys. 2019;103(3):747–757. doi:10.1016/j.ijrobp.2018.10.031 [PubMed: 30395906]
17. Wagenaar D, Tran LT, Meijers A, et al. Validation of linear energy transfer computed in a Monte Carlo dose engine of a commercial treatment planning system. Phys Med Biol. 2020;65(2):025006. doi:10.1088/1361-6560/ab5e97 [PubMed: 31801119]
18. Gu W, Ruan D, Zou W, Dong L, Sheng K. Linear energy transfer weighted beam orientation optimization for intensity-modulated proton therapy. Med Phys. Published online June 15, 2020. doi:10.1002/mp.14329
19. Gutierrez A, Rompokos V, Li K, et al. The impact of proton LET/RBE modeling and robustness analysis on base-of-skull and pediatric craniopharyngioma proton plans relative to VMAT. Acta Oncol Stockh Swed. 2019;58(12):1765–1774. doi:10.1080/0284186X.2019.1653496
20. Wang CC, McNamara AL, Shin J, et al. End-of-Range Radiobiological Effect on Rib Fractures in Patients Receiving Proton Therapy for Breast Cancer. Int J Radiat Oncol Biol Phys. 2020;107(3):449–454. doi:10.1016/j.ijrobp.2020.03.012 [PubMed: 32240774]
21. Guan F, Geng C, Ma D, et al. RBE Model-Based Biological Dose Optimization for Proton Radiobiology Studies. Int J Part Ther. 2018;5(1):160–171. doi:10.14338/IJPT-18-00007.1 [PubMed: 30338268]
22. Gu W, O'Connor D, Nguyen D, et al. Integrated Beam Orientation and Scanning-Spot Optimization in Intensity Modulated Proton Therapy for Brain and Unilateral Head and Neck Tumors. Med Phys. 2018;45(4):1338–1350. doi:10.1002/mp.12788 [PubMed: 29394454]
23. Gu W, Neph R, Ruan D, Zou W, Dong L, Sheng K. Robust beam orientation optimization for intensity-modulated proton therapy. Med Phys. 2019;46(8):3356–3370. doi:10.1002/mp.13641 [PubMed: 31169917]
24. Gu W, Ruan D, Zou W, Dong L, Sheng K. Linear energy transfer weighted beam orientation optimization for intensity-modulated proton therapy. Med Phys. 2021;48(1):57–70. doi:10.1002/mp.14329 [PubMed: 32542711]

25. Gu W, Ruan D, O'Connor D, et al. Robust optimization for intensity-modulated proton therapy with soft spot sensitivity regularization. Med Phys. 2019;46(3):1408–1425. doi:10.1002/mp.13344 [PubMed: 30570164]
26. Beck A, Teboulle M. A fast Iterative Shrinkage-Thresholding Algorithm with application to wavelet-based image deblurring. In: 2009 IEEE International Conference on Acoustics, Speech and Signal Processing.; 2009:693–696. doi:10.1109/ICASSP.2009.4959678
27. Malitsky Y, Pock T. A first-order primal-dual algorithm with linesearch. SIAM J Optim. 2018;28(1):411–432. doi:10.1137/16M1092015
28. Landers A, O'Connor D, Ruan D, Sheng K. Automated 4π radiotherapy treatment planning with evolving knowledge-base. Med Phys. 2019;46(9):3833–3843. doi:10.1002/mp.13682 [PubMed: 31233619]
29. Nguyen D, O'Connor D, Ruan D, Sheng K. Deterministic direct aperture optimization using multiphase piecewise constant segmentation. Med Phys. 2017;44(11):5596–5609. doi:10.1002/mp.12529 [PubMed: 28834556]
30. Boyd S. Distributed Optimization and Statistical Learning via the Alternating Direction Method of Multipliers. Found Trends® Mach Learn. 2010;3(1):1–122. doi:10.1561/2200000016
31. O'Connor D, Voronenko Y, Nguyen D, Yin W, Sheng K. Fast non-coplanar beam orientation optimization based on group sparsity. ArXiv171005308 Phys. Published online October 15, 2017. Accessed August 11, 2021. http://arxiv.org/abs/1710.05308
32. Chambolle A, Pock T. A First-Order Primal-Dual Algorithm for Convex Problems with Applications to Imaging. J Math Imaging Vis. 2011;40(1):120–145. doi:10.1007/s10851-010-0251-1
33. O'Connor D, Yu V, Nguyen D, Ruan D, Sheng K. Fraction-variant beam orientation optimization for non-coplanar IMRT. Phys Med Biol. 2018;63(4):045015. doi:10.1088/1361-6560/aaa94f [PubMed: 29351088]
34. Hueso-González F, Wohlfahrt P, Craft D, Remillard K. An open-source platform for interactive collision prevention in photon and particle beam therapy treatment planning. Biomed Phys Eng Express. 2020;6(5):055013. doi:10.1088/2057-1976/aba442 [PubMed: 33444244]
35. Huang S, Kang M, Souris K, et al. Validation and clinical implementation of an accurate Monte Carlo code for pencil beam scanning proton therapy. J Appl Clin Med Phys. 2018;19(5):558–572. doi:10.1002/acm2.12420 [PubMed: 30058170]
36. Cisternas E, Mairani A, Ziegenhein P, Jäkel O, Bangert M. matRad - a multi-modality open source 3D treatment planning toolkit. In: Jaffray DA, ed. World Congress on Medical Physics and Biomedical Engineering, June 7–12, 2015, Toronto, Canada. IFMBE Proceedings. Springer International Publishing; 2015:1608–1611. doi:10.1007/978-3-319-19387-8_391
37. Wieser HP, Cisternas E, Wahl N, et al. Development of the open-source dose calculation and optimization toolkit matRad. Med Phys. 2017;44(6):2556–2568. doi:10.1002/mp.12251 [PubMed: 28370020]
38. Grégoire V, Mackie TR. State of the art on dose prescription, reporting and recording in Intensity-Modulated Radiation Therapy (ICRU report No. 83). Cancer Radiother J Soc Francaise Radiother Oncol. 2011;15(6–7):555–559. doi:10.1016/j.canrad.2011.04.003
39. Trofimov A, Unkelbach J, DeLaney TF, Bortfeld T. Visualization of a variety of possible dosimetric outcomes in radiation therapy using dose-volume histogram bands. Pract Radiat Oncol. 2012;2(3):164–171. doi:10.1016/j.prro.2011.08.001 [PubMed: 22773939]
40. Ödén J, Eriksson K, Toma-Dasu I. Incorporation of relative biological effectiveness uncertainties into proton plan robustness evaluation. Acta Oncol. 2017;56(6):769–778. doi:10.1080/0284186X.2017.1290825 [PubMed: 28464736]
41. Wang L, Fossati P, Paganetti H, et al. The Biological Basis for Enhanced Effects of Proton Radiation Therapy Relative to Photon Radiation Therapy for Head and Neck Squamous Cell Carcinoma. Int J Part Ther. 2021;8(1):3–13. doi:10.14338/IJPT-20-00070.1 [PubMed: 34285931]
42. Nill S, Bortfeld T, Oelfke U. Inverse planning of intensity modulated proton therapy. Z Med Phys. 2004;14(1):35–40. doi:10.1078/0939-3889-00198 [PubMed: 15104008]
43. Wilkens JJ, Oelfke U. Analytical linear energy transfer calculations for proton therapy. Med Phys. 2003;30(5):806–815. doi:10.1118/1.1567852 [PubMed: 12772988]

44. Cao W, Lim GJ, Li Y, Zhu XR, Zhang X. Improved Beam Angle Arrangement in Intensity Modulated Proton Therapy Treatment Planning for Localized Prostate Cancer. Cancers. 2015;7(2):574–584. doi:10.3390/cancers7020574 [PubMed: 25831258]

45. Taasti VT, Hong L, Shim JS, Deasy JO, Zarepisheh M. Automating proton treatment planning with beam angle selection using Bayesian optimization. Med Phys. 2020;47(8):3286–3296. doi:10.1002/mp.14215 [PubMed: 32356335]

46. An Y, Shan J, Patel SH, et al. Robust intensity-modulated proton therapy to reduce high linear energy transfer in organs at risk. Med Phys. 2017;44(12):6138–6147. doi:10.1002/mp.12610 [PubMed: 28976574]

47. Bai X, Lim G, Wieser HP, et al. Robust optimization to reduce the impact of biological effect variation from physical uncertainties in intensity-modulated proton therapy. Phys Med Biol. 2019;64(2):025004. doi:10.1088/1361-6560/aaf5e9 [PubMed: 30523932]

48. Giantsoudi D. Can robust optimization for range uncertainty in proton therapy act as a surrogate for biological optimization? Int J Radiat Oncol Biol Phys. 2017;99(2):S106–S107. doi:10.1016/j.ijrobp.2017.06.253

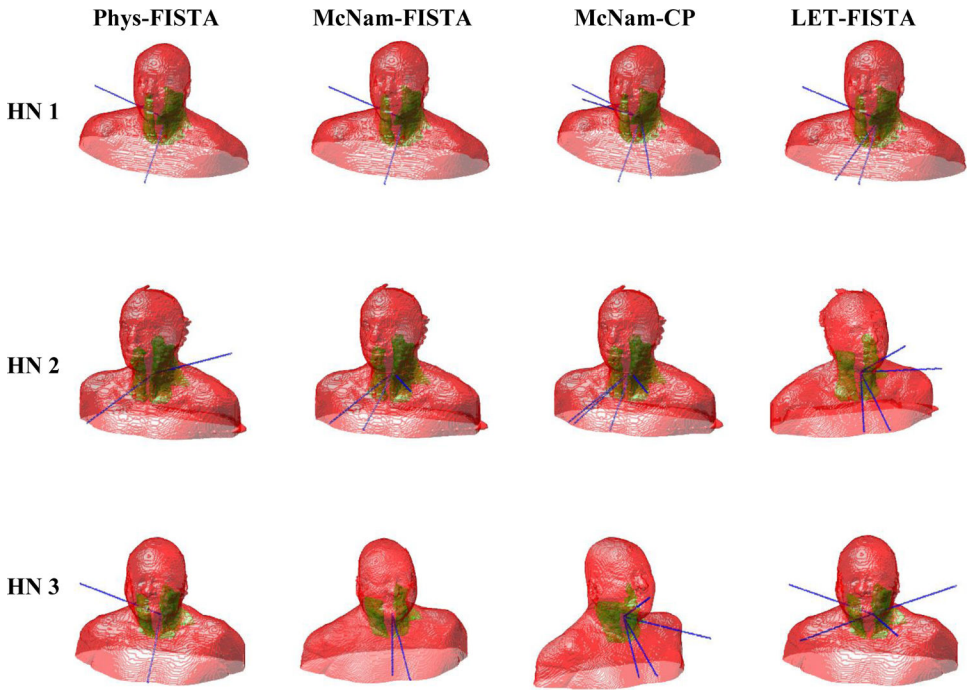

Figure 1.

Beam angle comparison between Phys-FISTA, McNam-FISTA, McNam-CP, and LET-FISTA (left to right) for all three patients. CTVs are shown in green and blue lines represent beams entering the patient.

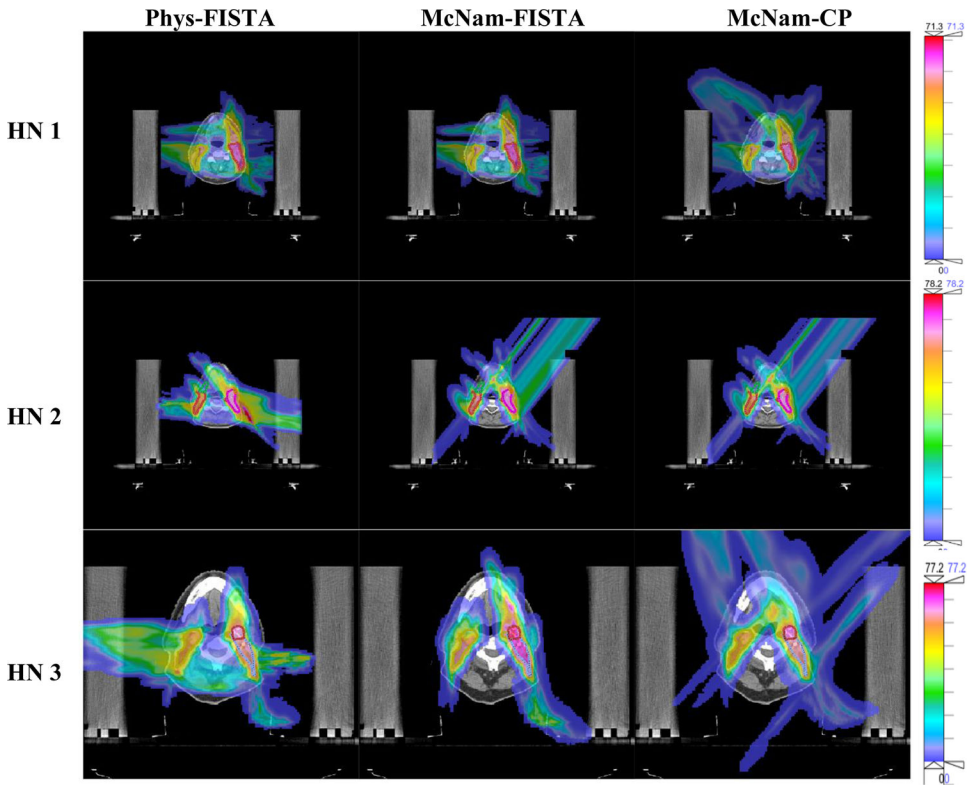

Figure 2.

Isodose comparison in the transverse plane between Phys-FISTA, McNam-FISTA, McNam-CP (left to right) for all three patients.

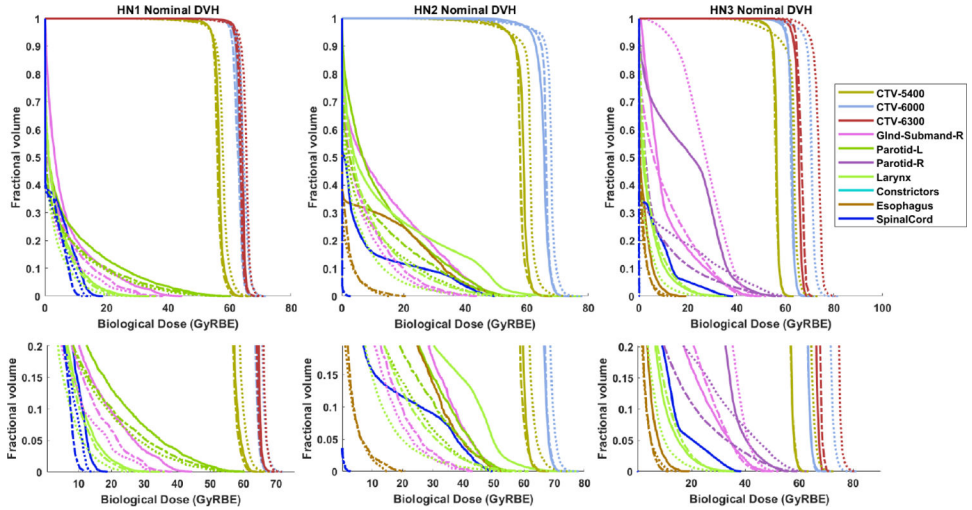

Figure 3.

Biological dose volume histograms for all patients. Solid lines represent Phys-FISTA, dotted lines represent McNam-FISTA and dashed lines represent McNam-CP. The bottom set of images is included as magnification of the above DVHs. Select structures are shown for each patient to portray the larger differences in dosimetry between plans.

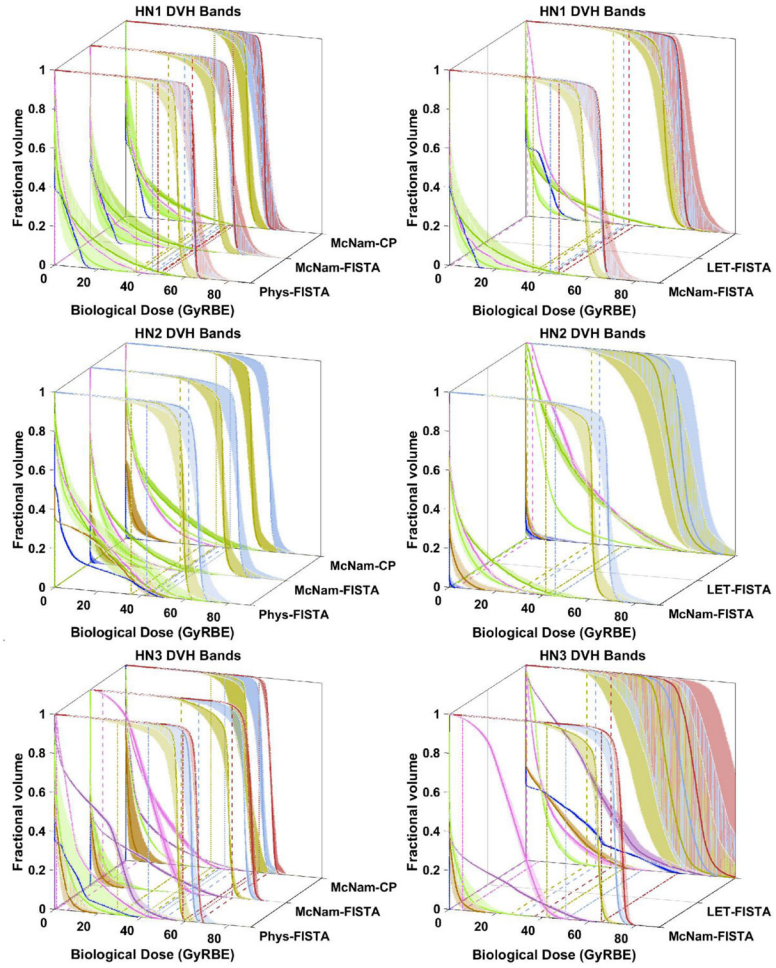

Figure 4.

DVH band plots for three H&N patients, indicating the robustness of the beams chosen by different methods. Worst case comparison for the McNamara plans compared to Phys-FISTA are shown on the left and comparison of McNam-FISTA with LET-FISTA are shown on the right. The worst D98% of each method is labeled by reference lines in the x-y plane. Select structures are shown on each subplot to portray the larger differences in robustness between plans.

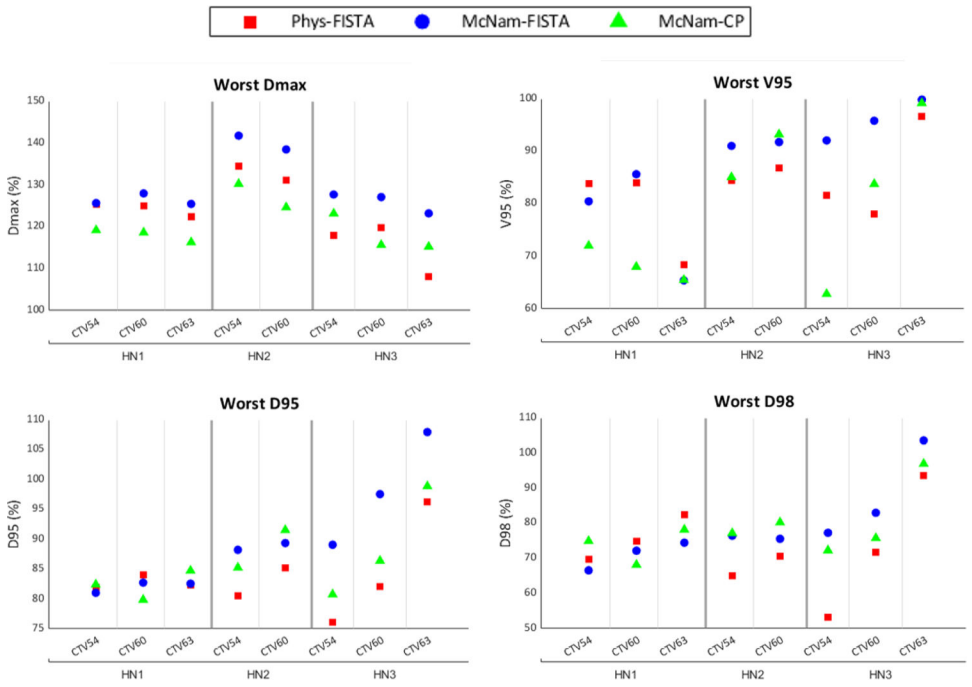

Figure 5.

A comparison of worst Dmax, V95%, D95%, and D98% of the CTVs for each patient under range and setup uncertainties between Phys-FISTA, McNam-FISTA, and McNam-CP. Doses and volume are shown as a percentage of the prescription dose and total volume.

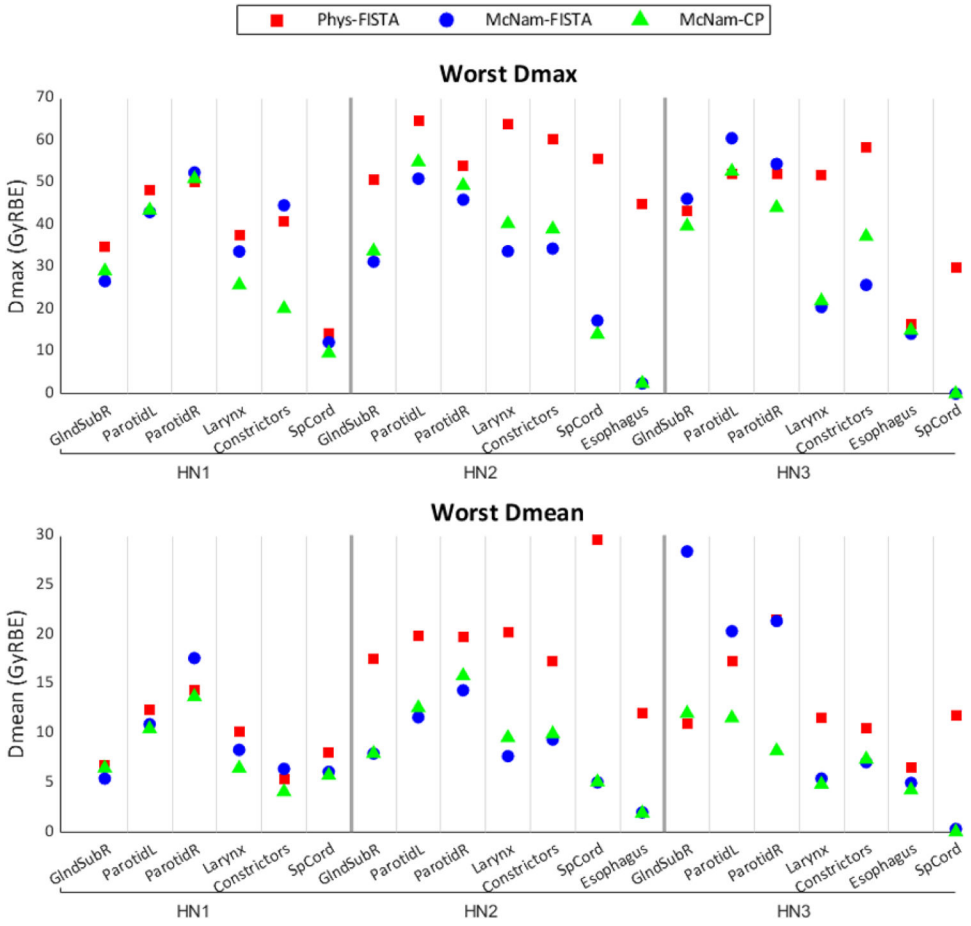

Figure 6.

Worst Dmax and Dmean for each OAR in each patient under various uncertainties between Phys-FISTA, McNam-FISTA, and McNam-CP. Dose values are given in GyRBE.

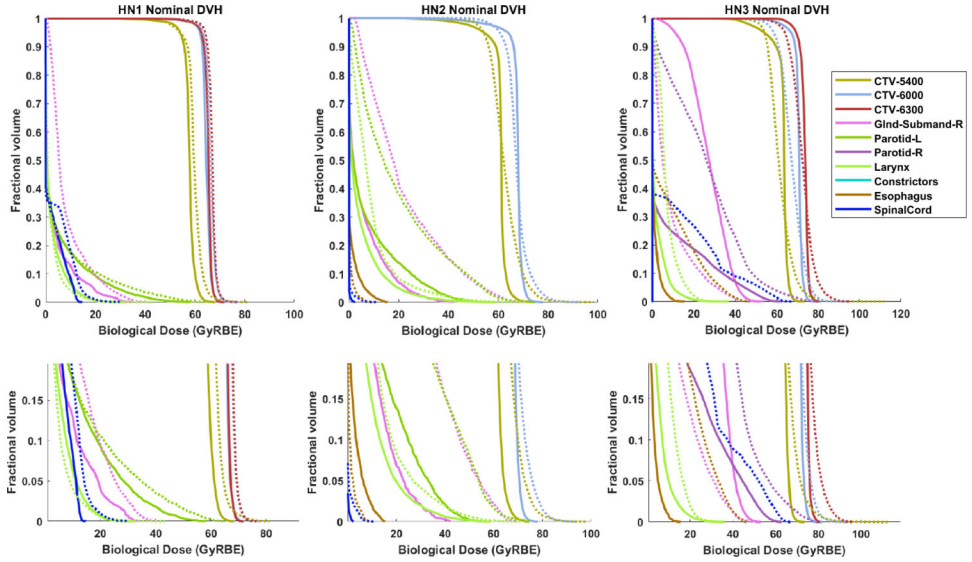

Figure 7.

Biological dose volume histograms for all patients. Solid lines represent McNam-FISTA and dotted lines represent LET-FISTA. The bottom set of images is included as magnification of the above DVHs. Select structures are shown for each patient to portray the larger differences in dosimetry between plans.

Table I.

Prescription doses, CTV volumes and average number of spots per beam for each patient.

Case		Prescription dose (GyRBE)	CTV volume (cc)	Average spots per beam
H&N 1	CTV54	54	141.29	10065
	CTV60	60	160.89	
	CTV63	63	68.00	
H&N 2	CTV54	54	108.00	10077
	CTV60	60	127.26	
H&N 3	CTV54	54	110.38	9433
	CTV60	60	98.94	
	CTV63	63	10.23	

Table II.

Preparation time and runtime of each SHBOO-FMO method for the tested patients.

	Calculation time (min)			SHBOO-FMO runtime (min)			
Case	**Dose**	**Sensitivity**	**Heterogeneity**	**Phys-FISTA**	**McNam-FISTA**	**McNam-CP**	**LET-FISTA**
H&N 1	51	4	682	24	55	247	44
H&N 2	63	7	700	19	88	95	93
H&N 3	43	3	690	10	51	147	45

Table III.

Beam angles (gantry, couch) in degrees selected for each patient.

	Beams Selected (gantry, couch)			
Case	**Phys-FISTA**	**McNam-FISTA**	**McNam-CP**	**LET-FISTA**
H&N 1	(270,18), (30, 88)	(270,18), (30, 88)	(311, 41), (270, 18), (37, 43), (30,88)	(270, 18), (324, 301), (30, 88)
H&N 2	(101, 342), (316, 314)	(36,0), (316, 314), (30, 88)	(36,0), (315, 314), (321,308), (31,76)	(33, 294), (54, 353), (324, 301), (30,88)
H&N 3	(270, 18), (30, 88)	(333, 297), (30, 88)	(329,52), (43,18), (321, 308), (328, 291)	(270, 18), (101, 342), (25, 346), (312, 352)

Table IV.

CTV statistic comparison between three methods for all patients. All biological dose values are reported in GyRBE. Best values are denoted in bold.

	HI			Dmax			D95%			D98%		
Case	**Phys-FISTA**	**McNam-FISTA**	**McNam-CP**	**Phys-FISTA**	**McNam-FISTA**	**McNam-CP**	**Phys-FISTA**	**McNam-FISTA**	**McNam-CP**	**Phys-FISTA**	**McNam-FISTA**	**McNam-CP**
HN #1												
CTV54	0.911	0.883	**0.921**	60.5	62.4	**59.8**	54.0	54.0	**54.0**	**52.3**	51.0	51.9
CTV60	**0.941**	0.925	0.932	65.6	68.0	**65.3**	61.2	62.0	**60.3**	**60.1**	59.8	59.3
CTV63	**0.948**	0.933	0.946	65.9	67.9	**65.6**	62.0	**62.6**	61.4	**60.9**	60.1	60.2
HN #2												
CTV54	0.877	0.842	**0.890**	62.5	66.2	**62.2**	**54.0**	**54.0**	**54.0**	**50.4**	46.6	47.9
CTV60	0.899	0.905	**0.919**	69.4	71.6	**69.3**	**61.6**	63.8	62.8	**58.2**	55.0	56.9
HN #3												
CTV54	**0.930**	0.817	0.928	**58.9**	67.1	59.1	**54.0**	**54.0**	**54.0**	**52.0**	46.3	51.5
CTV60	0.930	0.915	**0.937**	65.2	74.2	**65.1**	**59.9**	66.9	60.4	58.0	62.1	**59.1**
CTV63	0.930	0.914	**0.932**	**67.8**	76.6	69.3	**62.6**	69.2	64.0	61.0	66.5	**62.9**

Table V.

OAR statistics comparison between three methods for all patient under. RBExDmean (Dmean for simplification) and RBExDmax (Dmax) are reported in GyRBE. Best values are denoted in bold.

	HN #1			HN #2			HN #3		
	Phys-FISTA	**McNam-FISTA**	**McNam-CP**	**Phys-FISTA**	**McNam-FISTA**	**McNam-CP**	**Phys-FISTA**	**McNam-FISTA**	**McNam-CP**
Right subm. Gland									
Dmean	6.6	**3.4**	4.6	13.1	**5.5**	6.6	10.8	27.0	**10.5**
Dmax	34.8	**25.7**	28.6	47.2	**30.2**	32.6	39.7	43.9	**38.4**
Left Parotid									
Dmean	7.0	**5.1**	5.4	12.6	**7.2**	9.1	9.8	12.0	**8.7**
Dmax	44.7	**38.9**	40.9	46.8	**40.2**	46.0	**49.8**	56.8	52.1
Right Parotid									
Dmean	13.4	**12.1**	12.2	7.3	**5.9**	7.5	19.2	8.2	**6.8**
Dmax	**44.4**	46.2	45.1	44.5	**43.5**	47.9	46.2	51.4	**43.9**
Larynx									
Dmean	3.6	**2.3**	3.4	13.6	**4.4**	7.7	3.7	**2.1**	4.4
Dmax	20.0	**15.6**	18.5	54.5	**30.0**	39.6	20.5	**15.0**	21.3
Constrictors									
Dmean	3.2	**1.3**	3.2	8.7	**4.8**	6.4	4.3	**3.2**	5.8
Dmax	17.2	**11.8**	18.0	43.7	**33.1**	37.6	27.3	**24.2**	35.9
Esophagus	N/A	N/A	N/A						
Dmean				9.2	**1.0**	1.3	1.8	**1.0**	1.1
Dmax				46.3	**10.1**	11.1	10.5	7.8	**6.7**
Spinal Cord									
Dmean	3.2	2.5	**2.2**	6.0	**0.0**	**0.0**	4.1	**0.0**	**0.0**
Dmax	14.0	12.1	**9.5**	43.4	0.4	**0.3**	29.4	**0.0**	**0.0**